Earthquake Engineering & Structural Dynamics
The Journal of the International Association for Earthquake Engineering

EARTHQUAKE ENGINEERING & STRUCTURAL DYNAMICS
Earthquake Engng Struct. Dyn. 2014; **43**:77–96
Published online 9 July 2013 in Wiley Online Library (wileyonlinelibrary.com). DOI: 10.1002/eqe.2333

Envelope-based pushover analysis procedure for the approximate seismic response analysis of buildings

Marko Brozovič and Matjaž Dolšek*,†

Faculty of Civil and Geodetic Engineering, University of Ljubljana, Ljubljana, Slovenia

SUMMARY

An envelope-based pushover analysis procedure is presented that assumes that the seismic demand for each response parameter is controlled by a predominant system failure mode that may vary according to the ground motion. To be able to simulate the most important system failure modes, several pushover analyses need to be performed, as in a modal pushover analysis procedure, whereas the total seismic demand is determined by enveloping the results associated with each pushover analysis. The demand for the most common system failure mode resulting from the 'first-mode' pushover analysis is obtained by response history analysis for the equivalent 'modal-based' SDOF model, whereas demand for other failure modes is based on the 'failure-based' SDOF models. This makes the envelope-based pushover analysis procedure equivalent to the N2 method provided that it involves only 'first-mode' pushover analysis and response history analysis of the corresponding 'modal-based' SDOF model. It is shown that the accuracy of the approximate 16th, 50th and 84th percentile response expressed in terms of IDA curves does not decrease with the height of the building or with the intensity of ground motion. This is because the estimates of the roof displacement and the maximum storey drift due to individual ground motions were predicted with a sufficient degree of accuracy for almost all the ground motions from the analysed sets. Copyright © 2013 John Wiley & Sons, Ltd.

Received 20 September 2012; Revised 24 May 2013; Accepted 27 May 2013

KEY WORDS: envelope-based pushover analysis procedure; modal pushover analysis procedure; N2 method; approximate incremental dynamic analysis; failure-based SDOF model; reinforced concrete buildings

1. INTRODUCTION

The complexity of seismic response of structures has triggered the development of many simplified nonlinear procedures, which combine together nonlinear static (pushover) analysis of entire structure and response spectrum analysis (RSA) of a single-degree-of-freedom (SDOF) model. So-called basic pushover-based methods (e.g. the N2 method [1]), which involve a pushover analysis for an invariant distribution of lateral forces and inelastic response spectra, have been adopted in different regulatory documents (e.g. ASCE 41–06 [2], Eurocode 8 [3]).

Many variants of the pushover-based methods have been proposed. Adaptive spectra-based pushover analysis procedure was proposed by Gupta and Kunnath [4], where the load vectors are gradually updated. Aydinoglu [5] has argued that loading characteristics should be based on an inelastic rather than an elastic spectrum and has proposed an incremental RSA procedure. However, Antoniou and Pinho [6] concluded that current force-based adaptive pushover analysis offers a relatively minor advantage in comparison with basic pushover analysis, which utilizes an invariant

*Correspondence to: Matjaž Dolšek, Faculty of Civil and Geodetic Engineering, University of Ljubljana, Ljubljana, Slovenia.
†E-mail: mdolsek@fgg.uni-lj.si

force vector, and found that displacement-based adaptive pushover procedures can provide significantly improved predictions in comparison with existing force-based algorithms [7]. In the mean time, Chopra and Goel [8] introduced the modal pushover analysis (MPA) procedure, which involves several pushover analyses using the inertia force distribution for each mode. In the case of buildings, which behave linearly elastically, the MPA procedure is equivalent to well-known RSA (e.g. [9]). The latter followed a modified MPA (MMPA) procedure [10], in which the response contributions of the higher vibration modes are computed by assuming the building to be linearly elastic. Recently, Reyes and Chopra [11] extended MPA to the three-dimensional analysis of buildings subjected to two horizontal components of ground motions, whereas Kreslin and Fajfar [12] proposed the extended N2 method, which takes into account higher mode effects in elevation, and is consistent with the N2 method for plan-asymmetric buildings [13]. Additionally, Sucuoğlu and Günay [14] proposed the use of generalized force vectors for multi-mode pushover analysis. The generalized pushover analysis (GPA) procedure is based on enveloping the results associated with a sequence of pushover analyses, each performed to the target storey drift.

One of the few studies which partly addressed the question of the ability of the pushover-based method to predict seismic response of a structure due to a single ground motion was published by Bobadilla and Chopra [15]. They concluded that first-mode SDOF models can estimate the median roof displacement of reinforced concrete frame buildings to a useful degree of accuracy, whereas this may not be true in the case when the roof displacement is estimated for an individual ground motion. Pushover-based methods [16–19] are also used as an alternative to incremental dynamic analysis (IDA) [20], which provides response parameters for the full range of ground motion intensity levels, or for the support of a structure-specific selection of ground motions (e.g. [21–23]). Especially in the latter case the accuracy of a pushover-based method to predict seismic demand for individual ground motions become important.

This paper provides a description of a proposed envelope-based pushover analysis (EPA) procedure, which enables prediction of the seismic demand for each response parameter and for a particular ground motion by enveloping the results associated with three pushover analyses. The EPA procedure is presented in terms of approximate IDA. Its application is demonstrated by means of three reinforced concrete frame buildings, subjected to two sets of ground motions. Firstly, the background to approximate IDA and the procedure for pushover analysis are presented. Then, the differences between the modal-based and so-called failure-based SDOF models are emphasized, followed by a description of the proposed procedure, the response statistics and the error measures, which are then used to evaluate the accuracy of EPA-based approximate IDA curves.

2. PREDICTION OF APPROXIMATE IDA CURVES USING MODAL-BASED AND FAILURE-BASED SDOF MODELS

2.1. Background

The approximate procedures for the determination of IDA curves involve pushover analysis or several pushover analyses using a structural model of entire building (the so-called multi-degree-of-freedom (MDOF) model) and ‘exact’ or approximate IDA of one or several equivalent SDOF models [16, 17, 19, 24, 25]. According to basic pushover-based methods, approximate IDA curves can be determined by defining the distribution of the invariant lateral forces for pushover analysis, performing the pushover analysis, defining the transformation [1] or modification factor [2], which relate the displacement of the equivalent SDOF model to the roof displacement of the structural model, defining the SDOF model and performing IDA for this model using a set of ground motion records. The roof displacement of the structure is determined simply by multiplying the displacement of the SDOF model with the transformation (or modification) factor. The maximum storey drift given the specified ground motion intensity can be assessed by using the results of the pushover analysis that correspond to the known roof displacement.

Such a basic approach involves just one SDOF model, but results obtained in this way can be combined with the results of standard modal analysis (RSA) to approximately incorporate

DOI: 10.1002/eqe

the effects of 'higher modes' in elevation [12]. Another possibility is to perform several pushover analyses and assess the seismic responses for each corresponding SDOF model. In this case, the total demand can be achieved by combining together the corresponding structural responses by an appropriate modal combination rule, which leads to the MPA procedure [8, 11, 17]. Several SDOF models can also be used to approximately estimate the effects of modelling uncertainties [24, 25]. Although the fundamentals for the determination of the displacement demand of a SDOF model are the same for all the described procedures, the results may vary because of the definition of the distribution of the lateral forces for the pushover analysis, the transformation factor, the idealization of the pushover curve, as well as some other factors.

2.2. *Pushover analysis and the idealization of pushover curves*

Pushover analyses can be performed by using an invariant height-wise force distribution, which corresponds to the product of the diagonal mass matrix M and the ith natural vibration mode ϕ_i

$$s_i = \mathrm{M} \cdot \phi_i. \tag{1}$$

This is the most common approach, which is consistent with the basic pushover-based methods (e.g. [1, 18, 19]), which involve only the first vibration mode distribution of lateral forces ($i=1$). Additionally, second and third vibration mode distributions of lateral forces ($i=2$, 3) are used by analogy with the MPA procedure [8]. Based on results of pushover analyses, storey drifts and the estimated certain level of damage to individual structural elements can be directly assessed for a given roof displacement.

The pushover curves are idealized to define the force–displacement relationship of the equivalent SDOF model, which is used for evaluation of the target displacement. It has been shown before that a quadrilinear base shear – roof displacement relationship (Figure 1) can be considered sufficiently accurate for the description of the pushover curves of reinforced concrete buildings [19]. This assumption has also been used to develop a web application [19], which has been used in this paper for comparison purposes. An idealized pushover curve can be defined by two-dimensional parameters, for example by the roof displacement D_2 and the base shear F_2, and by 4 dimensionless parameters (r_v, r_h, μ_u, α) [19]

$$r_v = \frac{F_1}{F_2}, \quad r_h = \frac{D_1}{D_2}, \quad \mu_u = \frac{D_3}{D_2}, \quad \alpha = -\frac{k_{pc}}{k_1} \tag{2}$$

where the forces and displacements at characteristic points of the *F–D* relationship, the initial stiffness k_1 and post-capping stiffness k_{pc} are presented in Figure 1.

2.3. *Incremental dynamic analysis for modal-based and failure-based SDOF models*

Force–displacement relationships of the modal-based SDOF models ($F^* - D^*$) are determined by dividing the base shear F and roof displacement D of the idealized pushover curve by a

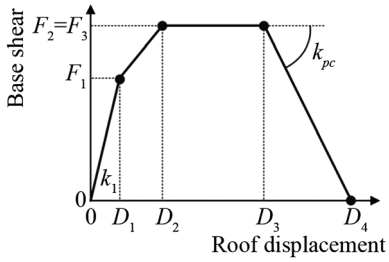

Figure 1. Idealized base shear – roof displacement relationship of a pushover curve.

DOI: 10.1002/eqe

transformation factor, which is defined by analogy with the N2 method [1] or, more generally, by analogy with MPA [8], as follows:

$$\Gamma_{m,i} = \frac{m^*_{m,i}}{\sum_{j=1}^{n} m_j \phi_{i,j}^2}, \quad m^*_{m,i} = \sum_{j=1}^{n} m_j \phi_{i,j} \tag{3}$$

where m_j is the jth storey mass, $\phi_{i,j}$ is the jth component of the ith natural vibration mode, which, in this paper, is always normalized to a roof displacement equal to 1, and $m^*_{m,i}$ is the mass of the modal-based SDOF model corresponding to the ith natural vibration mode. This is the commonly used definition of the transformation factor and mass of the SDOF model [1, 8], which are herein denoted by the index m, because $\Gamma_{m,i}$ is in fact the modal participation factor for the ith natural vibration mode. Because the quadrilinear relationship enables very good idealization of the first part of the pushover curve, when the structural behaviour is still elastic, the period of the so-called ith modal-based SDOF model

$$T^*_{m,i} = 2\pi \sqrt{\frac{m^*_{m,i} D_{1,i}}{F_{1,i}}} \tag{4}$$

is practically the same as the 'ith-mode' elastic period T_i of the structure. Note that in Equation (4) $D_{1,i}$ and $F_{1,i}$ correspond to the roof displacement and base shear at the first point (Figure 1) of the idealized ith-mode pushover curve, respectively.

Comparative studies have shown that modal-based SDOF models may not estimate roof displacement to a usefully degree of accuracy for an individual ground motion (e.g. [15]). In fact, the displacement demand of modal-based SDOF models is almost always governed by the first vibration mode (e.g. [17]). To improve the accuracy of prediction of the displacement demand and collapse capacity for an individual ground motion, so-called failure-based SDOF models are defined. These models are capable of approximately simulating roof displacement for those cases when the accuracy of the modal-based SDOF model associated with the first-mode pushover analysis is insufficient. The failure-based SDOF models utilize the displacement vectors corresponding to the system failure modes that are observed from pushover analyses (Section 2.2). In this paper, the system failure mode is associated with 80% strength in the softening branch of the ith-mode pushover curve. Note that a different definition of system failure modes, if associated with the inelastic displacement shape after the plastic mechanism had occurred, would not significantly affect estimates of the failure-based SDOF model, because the displacement shape does not change significantly once the plastic mechanism has formed. However, a brief discussion about this issue is given in Section 5.3.

Based on the earlier definition, the modal-based and failure-based SDOF models differ according to the definitions of the transformation factor and effective mass, which are in the case of failure-based SDOF models, defined as follows:

$$\Gamma_{f,i} = \frac{m^*_{f,i}}{\sum_{j=1}^{n} m_j d_{i,j}^2}, \quad m^*_{f,i} = \sum_{j=1}^{n} m_j d_{i,j} \tag{5}$$

where $d_{i,j}$ is the jth component of the normalized 'ith failure mode' displacement vector ($d_{i,n} = 1$) associated with the pushover analysis for the 'ith vibration mode' force distribution. Consequently, the period of the ith failure-based SDOF model

$$T^*_{f,i} = 2\pi \sqrt{\frac{m^*_{f,i} D_{1,i}}{F_{1,i}}} \tag{6}$$

can differ slightly in comparison with $T^*_{m,i}$, if a difference between $m^*_{f,i}$ and $m^*_{m,i}$ occurs. It should be noted that the normalized failure mode displacement vector, which correspond to the 'first-mode'

DOI: 10.1002/eqe

pushover curve, is very similar to the first natural vibration mode. For this reason modal-based and failure-based SDOF models are almost equal when they correspond to the first-mode pushover curve because $\Gamma_{f,1} \approx \Gamma_{m,1}$.

The force–displacement relationship used in the modal-based or failure-based SDOF model (F^*-D^*) is determined by dividing the idealized base shear – roof displacement by an appropriate transformation factor Γ. The hysteretic behaviour of the SDOF model should simulate the global response of a specific type of structure. It thus depends on the type of structure which is the subject of a seismic performance assessment. In this paper, the peak-oriented model is used to describe the cyclic behaviour of the SDOF model [19]. Note that it has already been shown that such a model is sufficiently accurate for the simulation of the global cyclic behaviour of reinforced concrete buildings (e.g. [25, 26]), provided that monotonic curves implicitly account for cyclic strength deterioration. An algorithm introduced by Vamvatsikos and Cornell [20] is used for computation of the exact IDA curves for both types of SDOF models.

The approximate IDA curves can be presented for different pairs of the intensity measure (IM) and the engineering demand parameter (EDP). The peak ground acceleration (a_g) and the spectral acceleration corresponding to the first mode period of the structure $S_a(T_1)$ are often used as ground motion IMs, whereas the maximum roof displacement (D_{max}) or roof displacement ratio (θ_{roof}) and the maximum storey drift ratio (θ_{max}) represent the EDP. Values for θ_{max} can be obtained from the results of pushover analysis on the basis of the known maximum roof displacement. In the case of the MPA procedure [8], the total demand in terms of the EDP is determined by an appropriate modal combination of the responses obtained in the case of each modal-based SDOF model [8, 17]. When, in this paper, the MPA is used, the modal responses are combined according to the square-root-of-sum-of-squares rule.

It should be noted, as mentioned earlier, that the approximate IDA curves, which correspond to a particular set of ground motions, can be estimated by a web application [19], which involves a query of the appropriate IDA curves from the response database and the *n*-dimensional linear interpolation. This approach is an alternative to the exact IDA for the SDOF model, which is obviously less accurate in comparison with a nonlinear response history analysis of the SDOF model, but nevertheless enables a rapid yet still sufficiently accurate prediction of approximate IDA curves [19].

2.4. Prediction of seismic demand by the proposed envelope-based pushover analysis procedure

The EPA procedure assumes that seismic demand for each response parameter is controlled by a predominant system failure mode, which may vary according to a ground motion. However, differences between the system failure modes due to the effects of ground motions can be significant for long-period (taller) buildings. This phenomenon can be simulated by the response history analysis. Pushover analysis can also be used for the approximate simulation of this effect, but, clearly, single pushover analysis, whether performed by taking into account an invariant force vector, an adaptive force vector or even an adaptive displacement vector, is not able to simulate the variability of sidesway failure modes because of the effects of ground motions. This can be achieved only by performing several pushover analyses to approximately simulate the most important system failure modes observed from the response history analysis.

The following additional assumptions are made to approximately simulate the most important system failure modes, the corresponding seismic demand and the total seismic demand:

(1) The most important failure modes can be simulated by pushover analyses by assuming invariant force distribution, which is determined on the basis of the first, second and third vibration modes (Equation (1)). Such an approach for the determination of pushover curves is equivalent to the MPA procedure [8]. However, it should be emphasized that the EPA procedure is not based on modal decomposition as is assumed in the case of the MPA procedure [8].
(2) The seismic demand for the first system failure mode is determined by using the modal-based SDOF model, which corresponds to the first vibration mode, and is defined by utilizing the transformation factor $\Gamma_{m,1}$. The demand associated with the second and third system failure modes is assessed by using a failure-based SDOF model ($\Gamma_{f,2}$ and $\Gamma_{f,3}$). The procedure for

DOI: 10.1002/eqe

determining the seismic demand corresponding to each pushover analysis is equivalent to that of the N2 method [1], provided that nonlinear response history analysis is used to determine the seismic demand of the SDOF models. A constant damping ratio is assumed for all the SDOF models. It should be noted that this is not consistent with the modal response history analysis (e.g. [9]). A further explanation is given in Section 5.3.

(3) The total seismic demand for each response parameter and for a particular ground motion is determined by enveloping the results associated with each pushover analysis. Such an approach does not require any combination of results or correction factors because each response parameter is directly determined from one of the three pushover analyses on the basis of the appropriate roof displacement.

2.5. *Response statistics and error measures*

The percentile IDA and corresponding approximate IDA curves are defined in this paper by linear interpolation between the closest percent ranks. If n ground motions are used, then the percent rank corresponding to kth sorted response parameter $y_1 \leqslant y_2 \leqslant \ldots \leqslant y_k \leqslant y_{k+1} \leqslant \ldots \leqslant y_n$ associated with the given ground motion intensity is defined as follows

$$p_k = \frac{100}{n}(k - 0.5) \tag{7}$$

The pth percentile response parameter y_p is defined as

$$y_p = \begin{cases} y_1 & \cdots \quad p < p_1 \\ y_n & \cdots \quad p > p_n \\ y_k + \dfrac{n}{100}(p - p_k)\left(y_{k+1} - y_k\right) & \cdots \quad p_k \leq p \leq p_{k+1} \end{cases} \tag{8}$$

Different error measures are used when discussing the accuracy of approximate procedures. The difference between the percentile IDA curve and the corresponding approximate IDA curve is assessed by the mean error between the limit-state intensities, which is defined by the expression

$$\varepsilon_p = \frac{100\%}{n_{ls}} \cdot \sum_{ls=1}^{n_{ls}} \frac{\left|IM_{p,\mathrm{appIDA}}(ls) - IM_{p,\mathrm{IDA}}(ls)\right|}{IM_{p,\mathrm{IDA}}(ls)} \tag{9}$$

where n_{ls} is the number of considered limit states and $IM_{p,\mathrm{IDA}}(ls)$ and $IM_{p,\mathrm{appIDA}}(ls)$ are the limit-state intensities corresponding to the pth percentile IDA and the approximate IDA (appIDA) curve, respectively.

The difference between the whole IDA curves is assessed by means of the normalized area between the two curves

$$\varepsilon_{IC} = 100\% \cdot \frac{\displaystyle\int_0^{EDP_{\max}(\mathrm{appIDA,IDA})} |\Delta IM| \mathrm{d}EDP}{\displaystyle\int_0^{EDP_{\max}(\mathrm{IDA})} IM_{\mathrm{IDA}} \mathrm{d}EDP} \tag{10}$$

where EDP is the maximum storey drift or roof displacement, IM corresponds to a_g or $S_a(T_1)$, ΔIM is the difference in the IM corresponding to the IDA and appIDA curves, IM_{IDA} is the IM of the IDA curve, EDP_{max}(appIDA,IDA) is the maximum of the EDPs corresponding to the capacity points of the appIDA and IDA curves, and EDP_{max}(IDA) is the engineering demand parameter corresponding to the capacity point of the IDA curve.

DOI: 10.1002/eqe

To investigate the accuracy of prediction for the storey drift ratios along the height of the building, an error measure is defined on the basis of the mean value of the normalized difference between the exact and approximate storey drift ratio, which is assessed over all the storeys and given intensity levels

$$\varepsilon_\theta = \frac{100\%}{n_i \cdot n_s} \cdot \sum_{i=1}^{n_i} \sum_{s=1}^{n_s} \frac{\left|\theta_{\text{appIDA}}(s,i) - \theta_{\text{IDA}}(s,i)\right|}{\max(\theta_{\text{IDA}}(i))} \tag{11}$$

where n_i is the number of intensities, which are uniformly distributed up to the minimum of the collapse capacity of the IDA and appIDA curves, n_s is the number of storeys of the examined building, $\theta_{\text{appIDA}}(s,i)$ and $\theta_{\text{IDA}}(s,i)$ are the storey drift ratios for the sth storey and the ith intensity, respectively, obtained by appIDA and IDA.

3. DESCRIPTION OF THE EXAMINED STRUCTURES, STRUCTURAL MODELS AND GROUND MOTIONS

3.1. Description of the structures

The 4-storey, 8-storey and 15-storey reinforced concrete frame buildings were investigated within the scope of this study (Figure 2). The 8-storey and 15-storey buildings were designed for earthquake resistance according to Eurocode 8 [3], whereas in the case of the 4-storey building, an earlier version of Eurocode 8 was used [28]. The seismic design parameters of the examined buildings and the strength class of the concrete and reinforcing steel are presented in Table I.

The dimensions of the cross section of the exterior columns and beams of the 4-storey building were 40/40 and 30/45 cm, respectively. The cross section of the inner column (45/45 cm) is slightly larger. The slab thickness was 15 cm. This building was designed for ductility class high. The model of the building was validated [27] on the basis of results of pseudodynamic tests performed at the ELSA laboratory [29]. The 8-storey building is symmetric in plan and regular in elevation. The cross sections dimensions of the columns and beams are 50/50 cm, and the slab thickness is 20 cm. The 15-storey building is a good representative of buildings whose seismic response is significantly affected by 'higher mode' effects in elevation. The dimensions of the cross section of the columns vary with the height of the building and amount to 70/80, 60/70 and 50/60 cm, respectively, for the columns of the 1st to 9th storeys, the 10th to 12th storeys and the 13th to top storey. All the beams have dimensions of 55/60 cm. Slab thickness is 22 cm. Four different concrete classes (Table I) were used in design. C40/50 was used in the first and second storeys. Concrete quality was first reduced in the third storey, then in the fifth and finally in the eight storey. Steel bars of quality class S500 were adopted in the design.

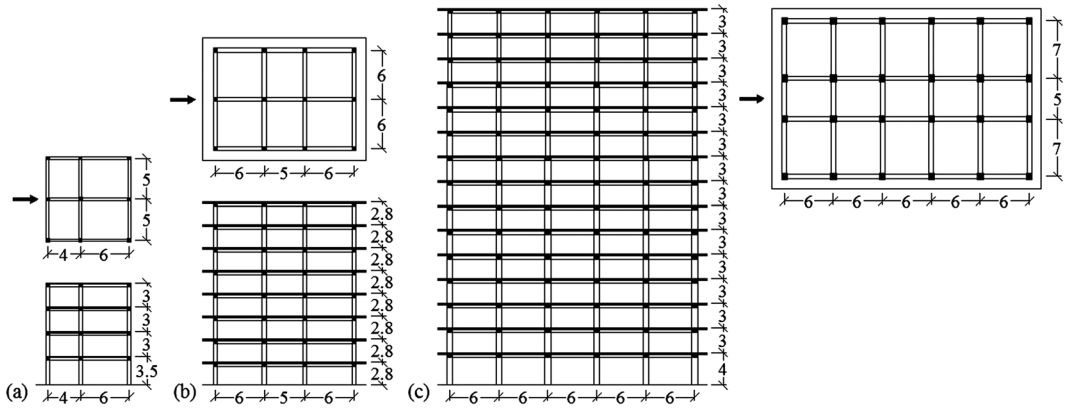

Figure 2. Elevation and plan views of (a) the 4-storey, (b) the 8-storey and (c) the 15-storey building, with the indicated direction of seismic loading.

DOI: 10.1002/eqe

Table I. The seismic design parameters of the buildings designed according to Eurocode 8.

Building	4-storey	8-storey	15-storey
Design ground acceleration (g)	0.3	0.25	0.25
Soil type	B	C	B
Ductility class	High	Medium	Medium
Behaviour factor	5	3.9	3.9
Concrete	C25/30	C30/37	C40/50, C35/45, C30/37, C25/30
Steel	B500	S500	S500

3.2. Description of the structural models

All the examined buildings were modelled as three-dimensional frame structures utilizing the PBEE toolbox [27] in conjunction with OpenSees [30]. A simplified nonlinear model was used. The floor diaphragms were assumed to be rigid in their own planes, and the masses and moments of inertia of each floor were lumped at the corresponding centre of gravity. The flexural behaviour of the beams and columns was modelled by one-component lumped plasticity elements, consisting of an elastic beam and two inelastic rotational hinges. The moment–rotation relationship before strength deterioration was modelled by a bilinear relationship, whereas post-capping stiffness was assumed to be negative and linear. Note that a schematic representation of the moment–rotation relationship in the plastic hinges of the columns and beams is presented later in the paper (Figure 6).

The yield and maximum moment in the columns were calculated on the basis of the moment–curvature analysis of the cross section by taking into account the axial forces due to the vertical loading. The ultimate rotation θ_u in the columns and beams corresponded to 80% of the maximum moment measured in the post-capping range of the moment–rotation relationship (the near collapse (NC) limit state). For columns θ_u was estimated by means of the Conditional Average Estimate (CAE) method [31]. In the case of the beams, EC8-3 [32] formulae were used to compute the ultimate rotations in the plastic hinges, a value of 1 being used for the parameter γ_{el}. Note that computation of the moment–rotation envelopes in plastic hinges is embedded in the PBEE toolbox [27]. The effects of deterioration under cyclic deformations were implicitly accounted for by the moment–rotation envelope, whereas the cyclic behaviour in the plastic hinges was simulated by using uniaxial hysteretic material available in OpenSees [30]. Because all the analysed structures are code-conforming, the effect of pinching was not simulated. The parameter β, which is used to define the degrading unloading stiffness, was assumed to have a value of 0.8. Such a model was calibrated several times against the experimental data from the full-scale pseudodynamic tests (e.g. [26, 27]). More details about the structural model are available elsewhere [27].

The geometric nonlinear ($P-\Delta$) effects were simulated for the overall building using a geometric transformation command [30] at the element level. The pushover or response history analysis was performed after the nonlinear static analysis, which simulated gravity loads on the beams and columns. Mass proportional damping was used for the nonlinear response history analyses. This damping model provided a seismic demand that was in between the demands obtained by using Rayleigh damping with initial stiffness and damping proportional to the instantaneous tangent stiffness. The damping constant was determined to give a 5% damping ratio at the fundamental period of vibration.

3.3. Description of the ground motions

The first set of ground motions (S1) consisted of 30 records [18]. All the ground motions corresponded to events with a magnitude between 6.5 and 6.9 and were obtained on soil having a shear–wave velocity in the upper 30 m of soil ($V_{s,30}$) larger than 180 m/s. The second set of ground motions (S2) consisted of 40 unscaled records corresponding to events with magnitudes of between 6.1 and 7.9. These records were selected so that their horizontal acceleration response spectra matched the median and variance of the predicted spectra for a magnitude 7 strike-slip earthquake at a distance of 10 km [33]. All these records were recorded on firm soil ($V_{s,30} > 180$ m/s). The acceleration spectra for each record for the sets S1 and S2, which were scaled to peak ground acceleration, as

DOI: 10.1002/eqe

well as the corresponding 16th, 50th and 84th percentiles, are presented in Figure 3. The basic data of the two sets of ground motions are available elsewhere [18, 34].

4. NATURAL VIBRATION PARAMETERS, PUSHOVER ANALYSIS AND THE CORRESPONDING SDOF MODELS

The natural vibration modes of the investigated buildings are presented in Figure 4. All the vibration modes have been normalized to the roof displacement. The fundamental vibration periods were 0.67, 1.23 and 1.90 s for the 4-storey, 8-storey and 15-storey buildings, respectively. The second and third vibration periods amounted from 31% to 35% and from 18% to 20% of the fundamental vibration periods, respectively.

The invariant force-based pushover analyses were performed for one orthogonal direction (Figure 2) for the three force distributions obtained by using Equation (1), with consideration of the first, second and third vibration modes (Figure 4). The pushover analyses were performed after the gravity load on the beams had been simulated. The roof displacement was monitored, using an increment of 0.005 m. Note that the geometric nonlinear (P−Δ) effects were taken into account as described in Section 3.2.

The maximum base shear versus weight ratio (F_b/W) for the first vibration mode force distribution amounted to 0.34, 0.11 and 0.07, respectively, for the 4-storey, 8-storey and 15-storey buildings (Table II). A substantial decrease in the base shear versus weight ratio, if assessed for the second-mode and third-mode pushover curves, was observed only in the case of the 4-storey building, whereas in the case of the other two buildings, the difference in strength due to the force distribution for pushover analysis was minor (Figure 5).

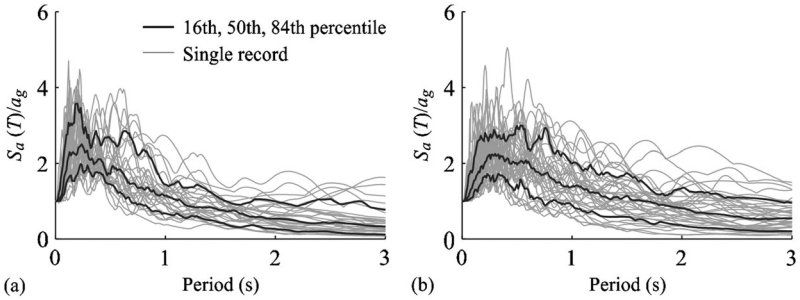

Figure 3. Acceleration spectra for single records and the corresponding 16th, 50th and 84th percentiles for the ground motion sets (a) S1 and (b) S2. The acceleration spectra are normalized to the peak ground acceleration.

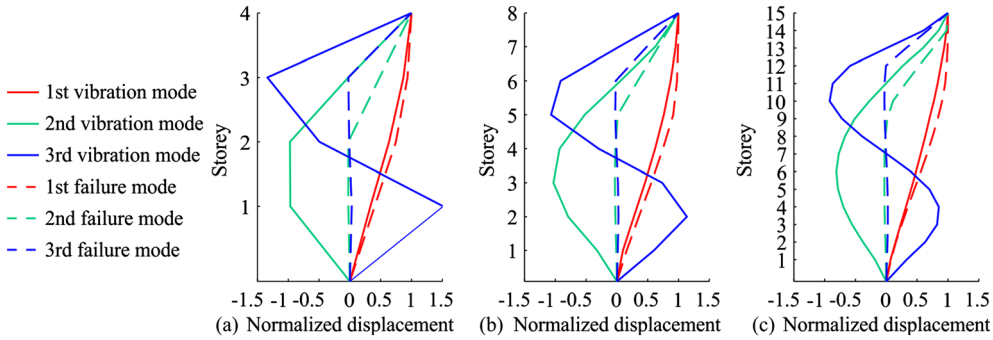

Figure 4. Normalized vibration modes and normalized failure modes of (a) the 4-storey, (b) the 8-storey and (c) the 15-storey building. The roof displacement is always equal to 1. The normalized failure modes correspond to 80% of the base shear force in the softening branch of the pushover curves.

DOI: 10.1002/eqe

Table II. The base shear versus weight ratio (F_b/W), the roof drift ratio ($\theta_{roof,NC}$), the maximum storey drift ratio ($\theta_{max,NC}$) corresponding to 80% strength in the softening branch of the pushover curve, and the period, mass, transformation factor and peak (yield) acceleration of the capacity diagram of the modal-based and failure-based SDOF models. The results are presented for all the investigated buildings and for the three pushover analyses performed for force distribution corresponding to the first, second and third vibration modes.

		Pushover analysis			Modal-based SDOF model				Failure-based SDOF model			
		F_b/W	$\theta_{roof,NC}$	$\theta_{max,NC}$	$T_m^* = T$	m_m^*	Γ_m	$S_{ay,m}$	T_f^*	m_f^*	Γ_f	$S_{ay,f}$
Building	Mode		(%)	(%)	(s)	(t)		(g)	(s)	(t)		(g)
4-storey	1	0.34	4.0	5.8	0.67	241	1.26	0.37	0.70	263	1.19	0.36
	2	0.26	2.6	5.7	0.21	87	0.35	2.80	0.25	120	1.16	0.61
	3	0.21	1.5	6.3	0.12	57	0.13	9.63	0.14	83	0.99	0.87
8-storey	1	0.11	2.7	4.3	1.23	1471	1.28	0.13	1.30	1664	1.19	0.13
	2	0.10	2.0	5.2	0.40	538	0.43	1.00	0.41	575	1.23	0.33
	3	0.11	1.3	5.1	0.23	372	0.24	2.71	0.25	446	1.20	0.45
15-storey	1	0.07	2.6	4.2	1.90	7010	1.35	0.08	2.00	7779	1.23	0.08
	2	0.06	1.5	5.3	0.67	2406	0.53	0.54	0.72	2729	1.20	0.21
	3	0.06	1.0	5.4	0.39	1549	0.30	1.49	0.39	1562	1.27	0.35

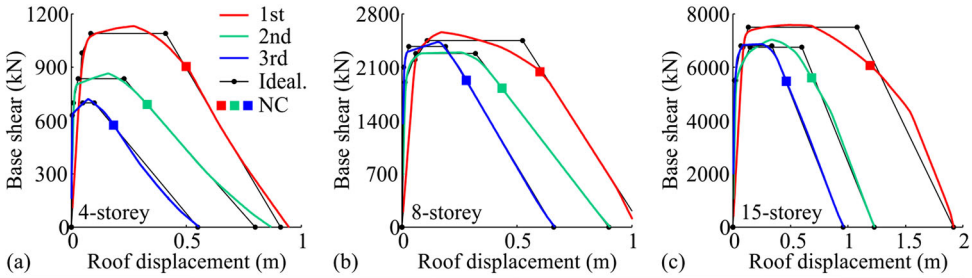

Mode	1st	2nd	3rd	1st	2nd	3rd	1st	2nd	3rd
F_2(kN)	1090	835	700	2450	2280	2370	7500	6750	6800
D_2(m)	0.09	0.03	0.05	0.11	0.06	0.03	0.14	0.15	0.07
r_v	0.90	0.84	0.90	0.90	0.83	0.89	0.90	0.81	0.81
r_h	0.55	0.31	0.08	0.52	0.23	0.25	0.65	0.17	0.20
μ_u	4.82	7.67	2.00	4.77	5.33	6.33	8.00	4.00	4.86
α	0.10	0.02	0.01	0.12	0.03	0.02	0.12	0.05	0.03

Figure 5. The first-mode, second-mode, third-mode pushover curves and the corresponding idealized base shear – roof displacement relationship for (a) the 4-storey, (b) the 8-storey and (c) the 15-storey building. The highlighted points correspond to 80% strength in the softening branch of the pushover curve and to the characteristic points of the idealized relationship. The parameters of the idealized base shear – roof displacement relationships are presented in the accompanying tables.

The roof drift ratio for the first-mode pushover curve, which is associated with the NC limit state ($\theta_{roof,NC}$) defined at 80% strength in the softening branch of the pushover curve, was the largest for the 4-storey building (4%), whereas in the case of the other buildings, it amounted to around 2.6%. The roof drift ratios for the second-mode and third-mode pushover curves and the NC limit state were significantly smaller (Table II). However, the maximum storey drift ratios ($\theta_{max,NC}$) were of the same order of magnitude regardless of the force vector used in the pushover analysis.

The damage patterns for the first-mode pushover curves of the three buildings are similar (Figure 6). Strength degradation (in the case of the 4-storey and 8-storey building) or yielding of the reinforcement (in the case of the 15-storey building) was observed in the columns at the base. Above this location, up to a certain storey, the columns remain undamaged. However, in the upper half of the buildings, yielding of the reinforcement was observed at the top of the columns in a certain storey, or in two consecutive storeys. Most of the beams suffered damage from yielding of the reinforcement up to the NC limit state.

DOI: 10.1002/eqe

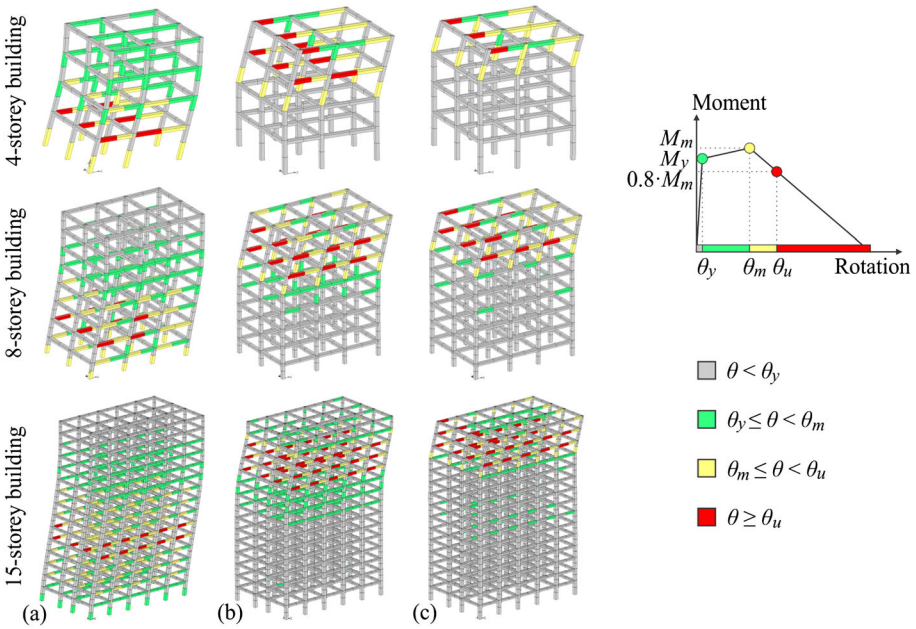

Figure 6. Deformed structures at the near collapse limit state with indications of the damage occurring to individual structural elements and typical moment–rotation relationship for columns and beams. The results are presented for (a) first-mode, (b) second-mode and (c) third-mode pushover analysis.

Damage associated with the second-mode pushover analyses was concentrated in the upper parts of the buildings, whereas in the lower parts of the structures, only minor damage was observed (Figure 6). However, this is even more evident in the case of damage corresponding to the third-mode pushover curves. Note that deformations along the height of the buildings followed the shape of second-mode or third-mode distribution of lateral forces, whereas the structure was still in the elastic range. After plastic mechanism has been formed, the deformations increased only in the damaged storeys, whereas the deformations of the other parts of the buildings gradually decreased because of the softening of the critical structural elements.

The modal-based and failure-based SDOF models for the first three modes were determined as defined in Section 2. In the case of EPA procedure, the mass proportional damping associated with a 5% damping ratio was assumed for all the SDOF models. Note that such approach is not consistent with the modal response history analysis (e.g. [9]). Further explanation regarding this assumption is given in Section 5.3.

The idealized base shear – roof displacement relationships for all the investigated buildings and pushover analyses are presented in Figure 5, where the corresponding values of the dimensionless parameters (Equation (2)), and the second characteristic point of the idealized pushover curves are also shown. Note that the initial stiffness of the modal-based SDOF model was equal to that obtained from the pushover curves. The periods of the modal-based SDOF models therefore coincide with the natural vibration periods of the buildings (Table II).

The mass $m^*_{m,i}$ and the transformation factor $\Gamma_{m,i}$ are presented in Table II. It can be observed that in the case of the modal-based SDOF models associated with the second and third vibration modes, these parameters are significantly smaller than the corresponding values of the parameters of the failure-based SDOF models. The failure-based SDOF models of the first-mode pushover curves and the corresponding modal-based SDOF models have practically the same characteristics. However, the mass of these failure-based SDOF models is slightly higher than those of the modal-based SDOF model, whereas the opposite is true for the participation factors. The peak yield accelerations $S_{ay,f}$ of the failure-based SDOF models, which correspond to the second-mode and third-mode pushover analysis, are significantly smaller than the corresponding $S_{ay,m}$ of the modal-based SDOF models (Table II). This indicates that the differentiation between the modal-based and failure-based SDOF models becomes significant when they correspond to the second and third-mode pushover curves. In

DOI: 10.1002/eqe

this case, the transformation factors $\Gamma_{f,2}$ and $\Gamma_{f,3}$ are significantly larger than $\Gamma_{m,2}$ and $\Gamma_{m,3}$. Their order of magnitude is about the same as $\Gamma_{f,1} \approx \Gamma_{m,1}$. It should be noted that such a definition of the failure-based SDOF models enables approximate simulation of the global seismic demand associated with failure modes that cannot be simulated by the modal-based SDOF models.

5. EVALUATION OF THE PROPOSED PROCEDURE FOR APPROXIMATE IDA

The results of the EPA procedure were evaluated using the results of the IDA, MPA-based approximate IDA and those obtained by the basic pushover-based procedure, which involves first-mode pushover analysis (PA1). In the case of all the approximate procedures, the seismic demand of the SDOF models was determined by the response history analysis. For comparison reasons, the web application [19], which currently supports response for only ground motion set S1, was also used for the determination of the PA1-based approximate IDA curves. In this paper, this procedure is denoted by PA1W.

The peak ground acceleration, which caused global dynamic instability of the structural model, was estimated according to IDA with an error of less than 2% g for all cases considering the different buildings and ground motions. Each response history analysis at the structural level or at the level of the equivalent SDOF model was performed by using the Newmark integration scheme ($\gamma_N = 0.5$, $\beta_N = 0.25$) and assuming an integration time step of 0.01 s.

The results of analyses were evaluated in terms of the 16th, 50th and 84th percentile IDA curves and on the basis of the IDA curves for a single ground motions. The error between the results of approximate IDA and IDA are discussed using the measures defined in Section 2.5.

5.1. *The 16th, 50th and 84th percentile IDA curves*

The approximate percentile IDA curves for all the investigated buildings and sets of ground motions are presented in Figure 7 and compared with the percentile IDA curves. The spectral acceleration at the first mode period of the building and the maximum storey drift ratio were used for the IM and EDP, respectively. It can be firstly observed that the difference in the results obtained by using the PA1 and PA1W procedure is practically negligible. This confirms the assumption that the web

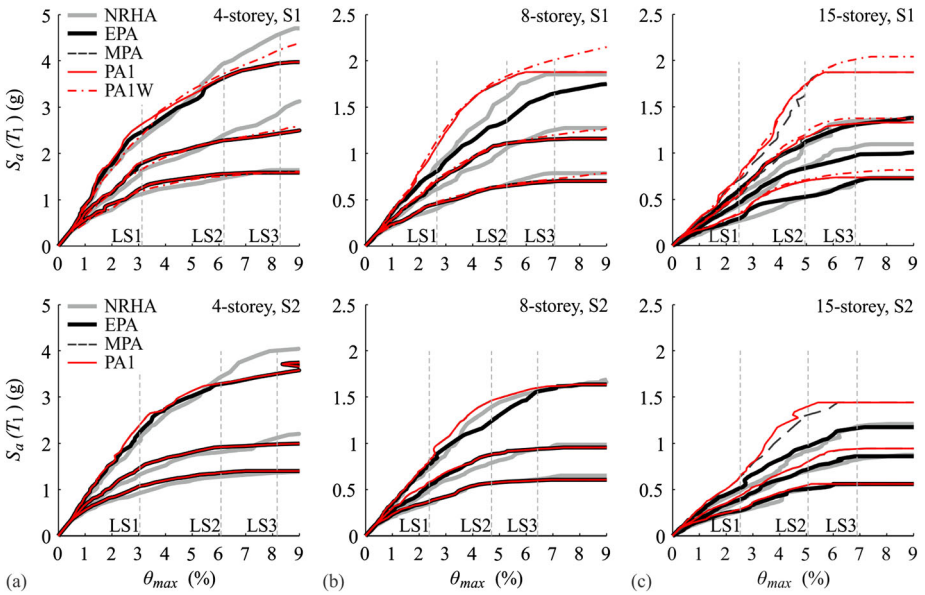

Figure 7. Comparison of 16th, 50th and 84th percentile IDA curves obtained by using NRHA and the approximate procedures denoted as PA1, PA1W (just for ground motion set S1), modal pushover analysis and envelope-based pushover analysis. The results are presented for the ground motions sets S1 and S2 and for the (a) 4-storey, (b) 8-storey and (c) 15-storey building. The vertical lines represent the engineering demand parameters at which the mean ε_p (Equation (9)) was assessed.

DOI: 10.1002/eqe

application provides sufficiently accurate estimates of IDA curves for SDOF models. However, the accuracy of the approximate IDA curves for SDOF models obtained by the web application depends on the idealization of the pushover curve and on the other parameters, which define the SDOF model. It is controlled by the parameter ρ [19], which was in the case of the presented examples in the interval between 0.83 and 0.87. On the basis of these values, it can be concluded that the web application predicted the expected mean error [19] for SDOF estimates of around 4%, which is in good agreement with the results presented in Figure 7 (see the difference between the PA1-based and PA1W-based approximate IDA curves when assessed for the ground motion set S1).

As expected, the approximate IDA curves for the 4-storey and 8-storey buildings were determined with acceptable accuracy. However, both of the approximate procedures, which utilize only the first-mode pushover curve, failed to predict the percentile IDA curves for the 15-storey building with an acceptable degree of accuracy. The largest difference was observed in the case of the 16th percentile IDA curves (Figure 7). A similar observation can be made if the percentile IDA curves are expressed with other combinations of IM and EDP.

The mean error (ε_p, Equation (9)), corresponding to three ($n_{ls} = 3$) arbitrarily defined EDPs, was assessed for comparison reasons to measure the ability of the approximate methods for predicting fractile IDA curves. The limit-state maximum storey drift ratio ($\theta_{max,LS}$) for the most severe limit state (LS3) corresponded to 85% of the maximum storey drift observed from the IDA curve for a single ground motion, whereas the limit-state storey drifts for LS2 and LS1 were defined, respectively, at 75% of the limit-state storey drift for LS3 and 50% of the limit-state storey drift for LS2. The limit-state maximum roof displacements ($D_{max,LS}$) were computed on the basis of the limit-state storey drifts for a single ground motion. The median limit-state storey drifts and roof displacements for a given ground motion set were then used to assess $IM_{p,\mathrm{IDA}}(ls)$ and $IM_{p,\mathrm{appIDA}}(ls)$ (Equation (9)). Note that the median limit-state storey drifts (Figure 7) differed with respect to the investigated buildings, and amounted from 2.4 to 3.1, from 4.7 to 6.2 and from 6.4 to 8.3, respectively, for LS1, LS2 and LS3. The results for the mean error ε_p, which was assessed for the fractile IDA curves expressed by different combinations of EDPs and IMs, are presented in Table III. These results confirm the conclusions of the earlier discussion. Clearly, ε_p increases significantly with respect to the 4-storey, 8-storey and 15-storey buildings for the approximate procedures except when it is assessed by the results of the EPA procedure. In general, ε_p is larger when it is based on the maximum storey drift ratio (θ_{max}). For most cases, a slightly smaller value of ε_p was observed for the ground motion set S2. An interesting result is that ε_p is the largest when assessed for the 16th percentile response and the smallest when assessed for the 84th percentile response. Additionally, the EPA procedure for an approximate IDA was able to predict the limit-state intensities with a useful degree of accuracy, even in the case of the 15-storey building.

5.2. *Comparison of the IDA curves for single ground motions*

The ability of the approximate procedures to generate an IDA curve for single ground motions was assessed by means of the parameters ε_{IC} and ε_θ (Equations (10) and (11)). Note that ε_{IC} is a measure of the difference between the two IDA curves, whereas ε_θ takes into account the ability of the pushover-based procedures to predict the maximum storey drift ratios along the buildings height and was in this paper assessed with consideration of 10 equidistant levels of the IM ($n_i = 10$, see Equation (11)).

For brevity, only the minimum, maximum and mean values of ε_{IC} are presented in Table IV, whereas ε_θ is reported also for each ground motion. The results indicate that ε_{IC} and ε_θ significantly depend on the ground motion (Table IV). The minimum of ε_{IC} did not exceed 6%. It is interesting that the minimum ε_{IC} did not increase because of the increased number of storeys. The opposite was observed in the case of the maximum ε_{IC} because the largest value was observed for the 15-storey building, whereas in the worst case, ε_{IC} amounted 250%. This error was induced by the PA1-based approximate IDA curve for the 11th ground motion from the set S1, which caused large ε_{IC} values for all the investigated buildings. Such large discrepancies were also observed in the case of some of the other ground motions from sets S1 and S2, regardless of the building under investigation. The EPA-based procedure for approximate IDA provided significantly smaller values for the maximum ε_{IC}. It is interesting that such an improvement did not significantly affect the mean value of ε_{IC} for the 4-storey and 8-storey buildings, but only the value for the 15-storey building.

DOI: 10.1002/eqe

Table III. The mean error ε_p assessed for the three limit-state intensities, the three investigated buildings, both sets of ground motions and different combinations of IMs (the peak ground acceleration a_g and the spectral acceleration at the first period $S_a(T_1)$) and the EDPs (the max. roof displacement D_{max} and the maximum storey drift ratio θ_{max}).

GM set S1		ε_p: 4-storey building				ε_p: 8-storey building				ε_p: 15-storey building			
		D_{max}		θ_{max}		D_{max}		θ_{max}		D_{max}		θ_{max}	
Procedure	Percentile	a_g	$S_a(T_1)$	a_g	$S_a(T_1)$	a_g	$S_a(T_1)$	a_g	$S_a(T_1)$	a_g	$S_a(T_1)$	a_g	$S_a(T_1)$
PA1	16th	11	10	14	12	24	4	35	12	18	22	62	45
	50th	4	7	8	11	7	9	8	9	14	13	19	29
	84th	5	7	6	7	6	10	4	9	5	4	16	23
PA1W	16th	10	3	13	5	28	9	41	17	21	20	66	47
	50th	4	3	5	7	6	8	7	9	16	17	20	33
	84th	6	5	8	4	5	10	5	9	6	5	19	28
MPA	16th	10	10	14	12	24	4	35	12	14	14	61	40
	50th	4	7	8	10	7	8	8	9	12	11	19	28
	84th	5	7	6	7	6	10	4	9	4	4	16	23
EPA	16th	11	10	9	9	11	6	4	12	12	3	7	5
	50th	4	7	8	10	7	9	8	9	13	6	7	6
	84th	5	7	6	7	6	10	4	9	5	4	5	4
GM set S2		ε_p: 4-storey building				ε_p: 8-storey building				ε_p: 15-storey building			
		D_{max}		θ_{max}		D_{max}		θ_{max}		D_{max}		θ_{max}	
Procedure	Percentile	a_g	$S_a(T_1)$	a_g	$S_a(T_1)$	a_g	$S_a(T_1)$	a_g	$S_a(T_1)$	a_g	$S_a(T_1)$	a_g	$S_a(T_1)$
PA1	16th	9	6	6	11	9	4	18	7	36	17	71	36
	50th	2	5	4	8	3	8	4	10	8	9	14	15
	84th	6	5	9	8	4	3	5	3	6	3	4	6
MPA	16th	9	6	6	11	8	4	18	7	28	15	62	32
	50th	2	5	4	8	3	8	4	10	8	8	14	15
	84th	6	5	9	8	4	3	5	3	6	3	4	6
EPA	16th	9	6	6	9	8	4	7	6	18	4	8	5
	50th	2	5	4	8	3	8	4	7	6	7	5	4
	84th	6	5	9	8	4	3	5	3	6	3	3	2

The differences between the minimum and maximum values of ε_θ are not so typical as those observed for ε_{IC}. The ε_θ values depend significantly on the ground motion record and gradually increase with the number of storeys of the building, which can be observed from the pattern presented by the background colours in Table IV, where ε_θ is presented for each ground motion from the two sets. In the case of the PA1-based procedure, 40% of the records from set S1 resulted in $\varepsilon_\theta > 25\%$ if they corresponded to the 4-storey building. This value increased to more than 80% in the case of the 15-storey building. Similar observations can be made in the case of ground motion set S2, but the ratio of the ground motions, which resulted in $\varepsilon_\theta > 25\%$, is smaller (from 13% to 63%). It is interesting that some ground motions caused ε_θ to occur in a 'red' zone regardless of the building under investigation. If $\varepsilon_\theta > 25\%$ occurred in the case of the 4-storey building or the 8-storey building, it is almost certain that the corresponding ground motion will cause the ε_θ to be in a 'red' zone for the 15-storey building. However, significantly smaller ε_θ values were observed on the basis of results obtained by the EPA procedure, which can be quickly seen from the pattern presented in Table IV and on the basis of the mean ε_θ. For almost all cases where ε_θ still exceeds 25% it has been shown that the EPA procedure provided results with greater accuracy than those estimated by the PA1-based procedure.

DOI: 10.1002/eqe

Table IV. The minimum, maximum and mean values of ε_{IC} and ε_θ according to the PA1 and EPA procedures for all the investigated buildings (4-storey (B4), 8-storey (B8) and 15-storey (B15)) and ground motion sets. The ε_θ values corresponding to each ground motion record are also presented, where light (yellow) and dark (red) backgrounds are used if $15\% \leqslant \varepsilon_\theta \leqslant 25\%$ and $\varepsilon_\theta > 25\%$, respectively.

	Ground motion set S1						Ground motion set S2					
	PA1			EPA			PA1			EPA		
ε_{IC} (%)	B4	B8	B15	B4	B8	B15	B4	B8	B15	B4	B8	B15
min	6	3	3	6	3	3	5	1	3	4	1	3
max	54	111	250	39	46	39	38	54	143	26	35	82
mean	15	17	45	14	13	17	11	12	29	10	11	17
ε_θ (%)												
min	9	10	8	9	9	7	7	6	6	8	7	5
max	39	39	39	26	28	24	35	40	38	37	27	29
mean	21	23	29	16	17	17	16	20	26	14	15	16
1	12	17	25	11	14	14	35	40	36	17	24	20
2	25	27	29	16	17	14	11	26	30	15	14	15
3	26	26	35	22	18	20	23	34	38	19	27	29
4	29	32	31	20	19	14	10	30	31	10	18	15
5	14	23	30	19	14	15	10	11	24	10	10	15
6	27	31	31	17	21	19	12	11	19	13	9	13
7	26	31	35	17	20	19	11	32	29	17	21	11
8	18	24	29	13	18	20	26	31	35	13	14	19
9	16	20	25	12	15	15	12	15	24	12	13	17
10	12	18	32	11	22	23	32	39	36	21	21	23
11	29	39	39	15	28	22	15	25	32	15	21	20
12	9	12	25	9	10	14	13	23	29	14	18	19
13	39	33	33	21	16	20	28	21	22	23	15	13
14	27	30	32	13	15	16	14	17	26	11	13	20
15	21	19	28	15	12	14	23	27	34	12	18	18
16	12	11	8	13	12	7	34	30	32	15	20	17
17	11	19	27	11	19	24	11	16	21	11	12	19
18	15	10	23	18	9	16	14	10	25	14	10	17
19	15	12	23	13	10	18	11	8	6	17	9	5
20	13	28	29	13	19	14	14	16	27	14	15	14
21	23	21	26	16	14	16	8	20	33	9	17	24
22	10	13	17	11	13	14	12	14	26	14	15	18
23	22	26	33	16	15	17	20	26	30	12	16	20
24	29	36	37	21	24	20	13	21	30	12	21	12
25	21	14	27	19	12	14	9	12	25	9	15	18
26	32	31	34	26	25	17	12	16	27	9	12	14
27	32	27	34	17	17	19	14	11	16	14	11	13
28	10	14	25	13	13	16	21	9	13	37	10	13
29	27	28	34	23	19	17	21	25	32	15	15	17
30	31	31	32	20	20	17	24	20	26	13	12	17
31							10	13	19	10	11	14
32							7	12	16	8	14	16
33							16	25	35	12	18	19
34							15	20	29	11	16	18
35							14	11	14	18	11	10
36							8	6	17	8	7	12
37							16	21	29	11	13	12
38							24	28	33	15	17	19
39							14	14	18	14	12	12
40							18	15	22	19	14	16

5.3. *Discussion of the results*

It has been demonstrated that for some ground motions the large differences occurred between the IDA curves and the approximate IDA curves when obtained by the PA1, PA1W or MPA procedures. Bobadilla and Chopra [15] observed the same phenomenon. A more detailed inspection of the results of this study can help to provide a better understanding of why such a discrepancy occurred. It was found that some ground motions caused very similar system failure modes in comparison with those obtained in the case of the first-mode pushover analysis. Typical representatives of such ground motions is ground motion No. 16 from set S1, and ground motion No. 19 from set S2 (for example, see ε_θ in Table IV). The approximate IDA curves for these ground motions, and for the 15-storey building, were predicted with a sufficient degree of accuracy even when obtained by the PA1 procedure. From Figure 8, it can be observed that the differences between the IDA curves and the corresponding approximate IDA curves when obtained on the basis of modal-based or failure-based SDOF models associated with the first-mode pushover analysis are practically negligible (these IDA curves overlap one another). The modal-based or failure-based

DOI: 10.1002/eqe

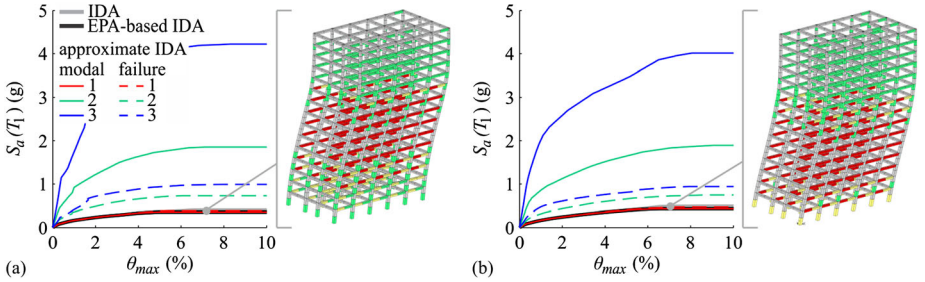

Figure 8. The IDA curves and the envelope-based pushover analysis based approximate IDA curves for the 15-storey building obtained for (a) ground motion No. 16 from set S1, and (b) ground motion No. 19 from set S2. In addition, the approximate IDA curves associated with the three modal-based and failure-based SDOF models are presented, together with the damage in the building close to the collapse capacity obtained by the NRHA.

SDOF models associated with the second-mode and third-mode pushover analysis do not affect the MPA-based or the EPA-based approximate IDA. This was expected because the damage to the building (Figure 8) obtained for an intensity level close to the collapse of the building is very similar to that obtained by first-mode pushover analysis.

However, some other ground motions caused a completely different type of damage to the building. For example, ground motion No. 1 from set S1 and ground motion No. 7 from set S2 (Figure 9) caused such damage to the 15-storey building, which was similar to that obtained in the case of second-mode and third-mode pushover analysis, respectively. From Figure 9(a), it can also be observed that the failure-based SDOF model associated with second-mode pushover analysis defined the EPA-based approximate IDA curve for intensities greater than 0.5 g. Similarly, the EPA-based approximate IDA curve for ground motion No. 7 from set S2 is controlled by the failure-based SDOF models associated with the second-mode and third-mode pushover analysis.

It was shown that the EPA procedure provided significantly improved estimates of the IDA curves, because it involves the failure-based SDOF models, which are capable of simulating different system failure modes, and not only the failure mode associated with the first-mode pushover analysis. However, it should be noted that invariant force-based pushover analysis may not be appropriate for the simulation of all system failure modes, which were observed from response history analysis. Namely, the damage in the building was, in the case of some ground motions, concentrated in the top part as well as in the lower part of the building, and also varied with respect of the level of intensity. Even in these cases, the EPA procedure proved to be sufficiently accurate or at least provided conservative estimates for the IDA curves, which was, for example, observed in the case of ground motion No. 24 from set S2 (Figure 10). Note that this ground motion from set S2 caused the maximum values of ε_{IC}, which were obtained by the EPA procedure (Table IV).

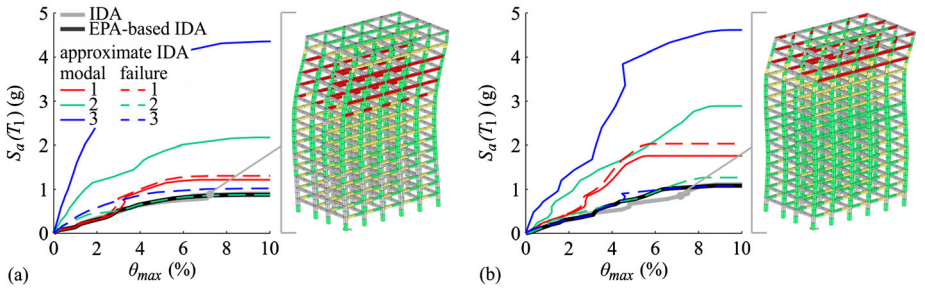

Figure 9. The IDA curves and the envelope-based pushover analysis based approximate IDA curves for the 15-storey building obtained for (a) ground motion No. 1 from set S1 and (b) ground motion No. 7 from set S2. In addition, the approximate IDA curves associated with the three modal-based and failure-based SDOF models are presented, together with the damage in the building close to the collapse capacity obtained by the NRHA.

DOI: 10.1002/eqe

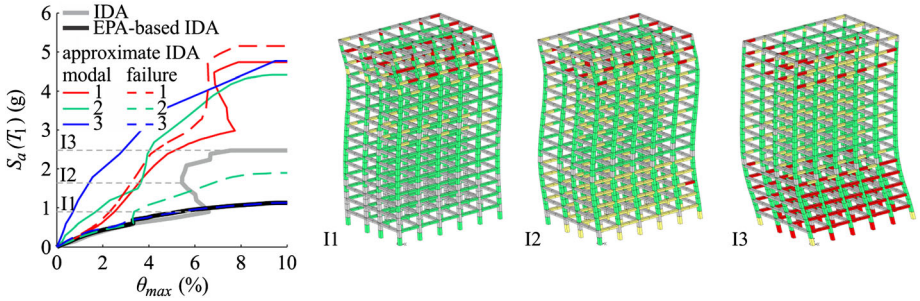

Figure 10. The IDA curve and the envelope-based pushover analysis based approximate IDA curve for the 15-storey building obtained for ground motion No. 24 from set S2. In addition, the approximate IDA curves associated with the three modal-based and failure-based SDOF models are presented, together with the damage in the building for selected levels of intensity obtained by the NRHA.

The ability of invariant force-based pushover analysis to predict appropriate system failure modes affects the estimation of storey drifts along the height of the building, because storey drifts according to the EPA procedure are directly determined by the envelope of storey drifts associated by the first-mode, second-mode and third-mode pushover analysis. Therefore, assessment of total demand, by using EPA procedure, does not involve any combination rule [8] or correction factors [12].

It has been observed that the EPA procedure predicted storey drifts in the upper part of the building with a useful degree of accuracy. For example, the storey drift ratios along the height of the 8-storey and 15-storey buildings are presented in Figure 11 for intensities associated with median IDA curves and the limit states LS1 and LS2 (Figure 7). The results based on EPA and nonlinear response history analyses are expressed in terms of the 16th, 50th and 84th

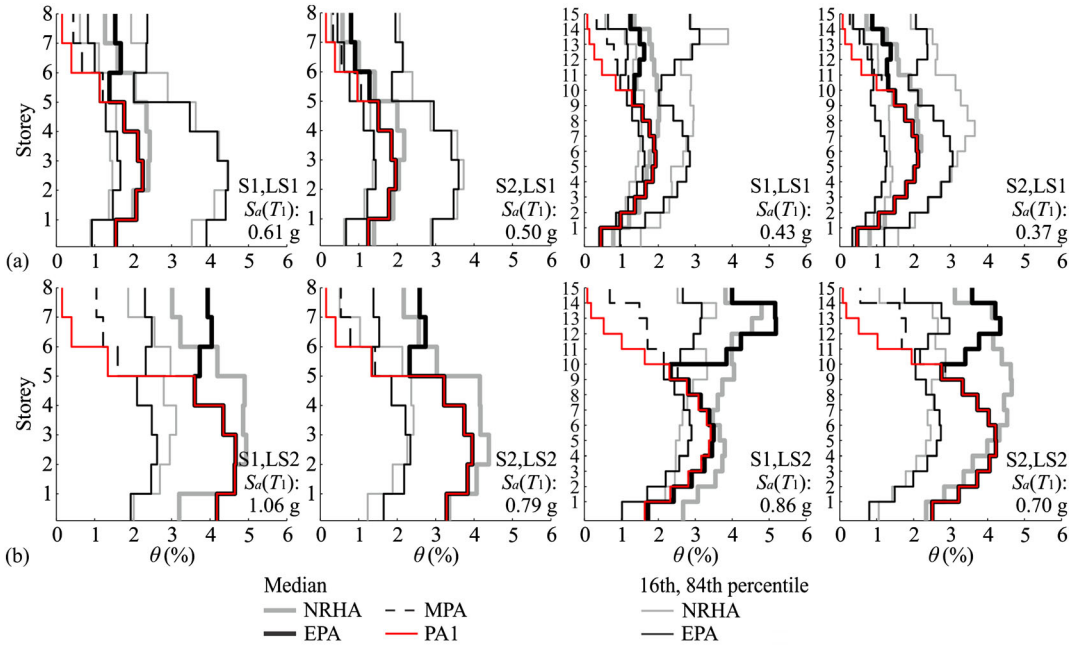

Figure 11. (a) The 16th, 50th and 84th percentile storey drift ratios for the 8-storey and 15-storey buildings and for the intensity associated with LS1 and the median IDA curve (Figure 7), and (b) the 16th and 50th percentile storey drift ratios for the same buildings associated with the limit state LS2 and the median IDA curve. The results are presented for both ground motion sets. The EPA-based storey drift ratios are compared with those of the nonlinear response history analysis, whereas only the median storey drift ratios are presented in the case of the modal pushover analysis and PA1 procedures. The 84th percentile storey drift ratios for the intensity associated with LS2 could not be presented since collapse of the buildings was predicted by the NRHA and the envelope-based pushover analysis procedure.

DOI: 10.1002/eqe

percentiles. Note that the 84th percentile storey drift ratios could not be presented for the intensities associated with LS2, because they corresponded to the collapse of building, which was also predicted by the EPA procedure.

Additionally, the median storey drifts assessed by the MPA and the PA1 procedure are presented. It can be observed that all three approximate methods provided similar results up to a certain storey, whereas the EPA procedure has the ability to improve the prediction of storey drifts in the upper part of the building. However, the storey drift ratios in some storeys are still systematically underestimated. This is the consequence of the inadequacy of invariant pushover analysis to simulate the most important system failure modes. For this reason, it is not possible to exclude the possibility that some other force vectors (e.g. [14]) may provide even better estimates for storey drifts along the height of the buildings.

In Figures 8 to 10, the IDA curves associated with the three modal-based and failure-based SDOF models are also presented. Some small differences can be observed for the IDA curves obtained by the modal-based or failure-based SDOF models associated with first-mode pushover analysis. Consideration of the failure-based SDOF model even for the first-mode pushover analysis would therefore not significantly affect the results of the EPA-based procedure. However, the demand of the failure-based SDOF model when associated with first-mode pushover analysis is slightly smaller than that of the corresponding modal-based SDOF model, which was also used in the EPA procedure. This is because the transformation factor $\Gamma_{f,1}$ is slightly smaller than the transformation factor $\Gamma_{m,1}$.

The opposite was observed in the case of the failure-based SDOF models associated with second-mode and third-mode pushover analysis. It should be noted that $\Gamma_{f,i}$ for $i=2$ and 3 increased gradually compared with $\Gamma_{m,i}$, if the $\Gamma_{f,i}$ were assessed on the basis of damaged structures. Such a trend was observed until the reinforcement in the columns started to yield, whereas $\Gamma_{f,i}$ for $i=2$ and 3 reached values of around 1. In the case of the deformation vector associated with the maximum base shear force and beyond the corresponding deformations, the $\Gamma_{f,i}$ values were more or less constant. Therefore, even in more general case, when it can be assumed that $\Gamma_{f,i}$ is a function of the displacement demand, the EPA-based approximate IDA curves would not be significantly affected, because Γ_f is more or less constant in the moderate and severe nonlinear range, which is the subject of interest.

An additional parameter which affects the seismic demand of the SDOF model is damping. In the EPA procedure, it is assumed that the damping ratio is the same for all three SDOF models. This is not consistent with the modal response history analysis, which is based on the use of an equal damping coefficient $a_0=2\xi_i\omega_i$ for all considered modes. However, decisions regarding the assumptions embedded in the EPA procedure are based on extensive parametric studies. It is very likely that the accuracy of the overall results would be reduced if the failure-based SDOF models would be based on different $\Gamma_{f,i}$ and the equal damping coefficient a_0 for all considered SDOF models. For illustration, the seismic response of the 15-storey building subjected to ground motion No. 4 from set S1 is presented in terms of an IDA curve (Figure 12) for several variations of the

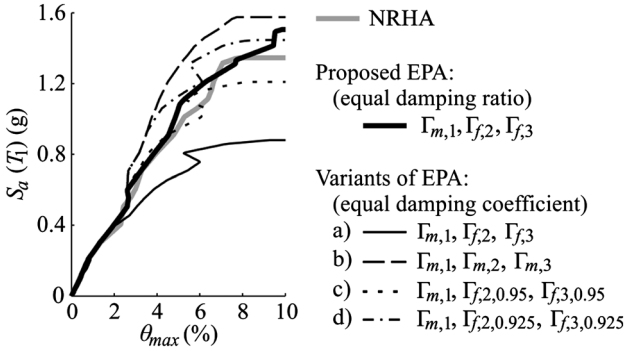

Figure 12. The IDA curve, the envelope-based pushover analysis based approximate IDA curve and the variants of the envelope-based pushover analysis based approximate IDA curves for the 15-storey building and ground motion No. 4 from set S1.

DOI: 10.1002/eqe

EPA procedure. If the EPA procedure were to be based on an equal damping coefficient a_0, then the seismic demand would be overestimated (variant a) in Figure 12). The other 'boundary' variant of the EPA procedure would involve the modal-based SDOF models, each having the same damping coefficient a_0 (variant b) in Figure 12). In this case, the SDOF model associated with the first pushover analysis would always define the target EDP. Variants c) and d) of the EPA procedure, which are presented in Figure 12, utilize the same damping coefficient a_0 for all SDOF models, but the transformation factors $\Gamma_{f,2}$ and $\Gamma_{f,3}$, which are obtained by using a displacement shape corresponding to 95% or 92.5% of the maximum strength from the pushover curves before the capping point. The corresponding results are closer to the results of the proposed EPA procedure, but are very sensitive, because variation of the displacement shape in the range close to the maximum strength is large. Additionally, the accuracy of results based on variants c) and d) depends significantly on the ground motion under consideration.

6. CONCLUSIONS

An EPA procedure has been proposed. It involves several pushover analyses to simulate the most important system failure modes and introduces so-called failure-based SDOF models, which are appropriate for assessing the seismic demand associated with 'higher' system failure modes. The proposed procedure does not involve a combination of modal responses or correction factors because the total demand for each of the response parameters is based on the enveloping results associated with each pushover analysis. The proposed procedure can be interpreted as a variant of the N2 method provided that the displacement demand of the equivalent SDOF model is determined by response history analysis.

The EPA assumes that each response parameter is affected by a predominant system failure mode. By means of several examples it has been shown that this assumption is quite appropriate since the system failure mode obtained by the nonlinear response history analysis is similar to the predominant system failure mode obtained by the EPA. An interesting result is that some ground motions always caused a response of buildings, which can be simulated by consideration of only 'first-mode' pushover analysis, regardless of the building under investigation. Quite the opposite was observed in the case of some other ground motions, because the total demand in terms of the EPA-based IDA curves was obtained on the basis of a 'higher mode' pushover analysis or several pushover analyses, depending on the ground motion intensity level.

It was shown that proposed procedure enables the sufficiently accurate prediction of IDA curves for single ground motions and consequently of fractile IDA curves. The accuracy of the EPA-based approximate IDA curves did not vary significantly with respect to the investigated buildings, ground motions or intensity level. Additionally, EPA provided estimates of storey drift along the elevation of the buildings with a useful degree of accuracy. It was shown that the fundamental system failure mode always controlled the storey drifts in the lower part of the buildings, whereas in the upper storeys, 'higher' system failure modes prevailed. However, the accuracy of prediction of storey drifts also depends on the ability of pushover analyses to simulate the most important system failure mode.

ACKNOWLEDGEMENTS

The results presented in this paper are based on work supported by the Slovenian Research Agency. This support is gratefully acknowledged. The authors greatly appreciate the constructive comments of anonymous reviewers, which contributed to improvements of the initial paper.

REFERENCES

1. Fajfar P. A nonlinear analysis method for performance-based seismic design. *Earthquake Spectra* 2000; **16**(3):573–592. DOI: 10.1193/1.1586128.
2. ASCE. Seismic rehabilitation of existing buildings, ASCE/SEI 41–06. American Society of Civil Engineers. 2007.
3. CEN. Eurocode 8: design of structures for earthquake resistance - part 1: general rules, seismic actions and rules for buildings, EN 1998–1. European Committee for Standardisation: Brussels, 2004.

4. Gupta B, Kunnath SK. Adaptive spectra-based pushover procedure for seismic evaluation of structures. *Earthquake Spectra* 2000; **16**(2):367–392. DOI: 10.1193/1.1586117.
5. Aydinoğlu MN. An incremental response spectrum analysis procedure based on inelastic spectral displacements for multi-mode seismic performance. *Bulletin of Earthquake Engineering* 2003; **1**(1):3–36.
6. Antoniou S, Pinho R. Advantages and limitations of adaptive and non-adaptive force-based pushover procedures. *Journal of Earthquake Engineering* 2004; **8**(4):497–522. DOI: 10.1080/13632460409350498.
7. Antoniou S, Pinho R. Development and verification of a displacement-based adaptive pushover procedure. *Journal of Earthquake Engineering* 2004; **8**(5):643–661. DOI: 10.1080/13632460409350504.
8. Chopra AK, Goel RK. A modal pushover analysis procedure for estimating seismic demands for buildings. *Earthquake Engineering and Structural Dynamics* 2002; **31**(3):561–582. DOI: 10.1002/eqe.144.
9. Chopra AK. *Dynamics of Structures: Theory and Applications to Earthquake Engineering* (3rd edn), Section 13.1. Prentice-Hall: Englewood Cliffs, NJ, 2007.
10. Chopra AK, Goel RK, Chintanapakdee C. Evaluation of a modified MPA procedure assuming higher modes as elastic to estimate seismic demands. *Earthquake Spectra* 2004; **20**(3):757–778. DOI: 10.1193/1.1775237.
11. Reyes CJ, Chopra AK. Three-dimensional modal pushover analysis of buildings subjected to two components of ground motion, including its evaluation for tall buildings. *Earthquake Engineering and Structural Dynamics* 2011; **40**(7):789–806. DOI: 10.1002/eqe.1060.
12. Kreslin M, Fajfar P. The extended N2 method taking into account higher mode effects in elevation. *Earthquake Engineering and Structural Dynamics* 2011; **40**(14):1571–1589. DOI: 10.1002/eqe.1104.
13. Fajfar P, Marušič D, Peruš I. Torsional effects in the pushover-based seismic analysis of buildings. *Journal of Earthquake Engineering* 2005; **9**(6):831–854. DOI:10.1080/13632460509350568.
14. Sucuoğlu H, Günay MS. Generalized force vectors for multi-mode pushover analysis. *Earthquake Engineering and Structural Dynamics* 2011; **40**(1):55–74.
15. Bobadilla H, Chopra AK. Evaluation of the MPA procedure for estimating seismic demands: RC-SMRF buildings. *Earthquake Spectra* 2008; **24**(4):827–845. DOI: 10.1193/1.2945295.
16. Dolšek M, Fajfar P. Simplified non-linear seismic analysis of infilled concrete frames. *Earthquake Engineering and Structural Dynamics* 2005; **34**(1):49–66. DOI: 10.1002/eqe.411.
17. Han SW, Chopra AK. Approximate incremental dynamic analysis using the modal pushover analysis procedure. *Earthquake Engineering and Structural Dynamics* 2006; **35**(15):1853–1873. DOI: 10.1002/eqe.605.
18. Vamvatsikos D, Cornell CA. Direct estimation of the seismic demand and capacity of oscillators with multi-linear static pushovers through IDA. *Earthquake Engineering and Structural Dynamics* 2006; **35**(9):1097–1117. DOI: 10.1002/eqe.573.
19. Peruš I, Klinc R, Dolenc M, Dolšek M. A web-based methodology for the prediction of approximate IDA curves. *Earthquake Engineering and Structural Dynamics* 2013; **42**(1):43–60. DOI: 10.1002/eqe.2192.
20. Vamvatsikos D, Cornell CA. Incremental dynamic analysis. *Earthquake Engineering and Structural Dynamics* 2002; **31**(3):491–514. DOI: 10.1002/eqe.141.
21. Azarbakht A, Dolšek M. Prediction of the median IDA curve by employing a limited number of ground motion records. *Earthquake Engineering and Structural Dynamics* 2007; **36**(15):2401–2421. DOI: 10.1002/eqe.740.
22. Azarbakht A, Dolšek M. Progressive incremental dynamic analysis for first-mode dominated structures. *Journal of Structural Engineering* 2011; **137**(3):445–455. DOI: 10.1061/(ASCE)ST.1943-541X.0000282.
23. Kalkan E, Chopra AK. Modal-pushover-based ground-motion scaling procedure. *Journal of Structural Engineering* 2011; **137**(3):298–310. DOI: 10.1061/(ASCE)ST.1943-541X.0000308.
24. Fragiadakis M, Vamvatsikos D. Fast performance uncertainty estimation via pushover and approximate IDA. *Earthquake Engineering and Structural Dynamics* 2010; **39**(6):683–703. DOI: 10.1002/eqe.965.
25. Dolšek M. Simplified method for seismic risk assessment of buildings with consideration of aleatory and epistemic uncertainties. *Structure and Infrastructure Engineering* 2012; **8**(10):939–953.
26. Fajfar P, Dolšek M, Marušić D, Stratan A. Pre-and post-test mathematical modelling of a plan-asymmetric reinforced concrete frame building. *Earthquake Engineering and Struc. Dynamics* 2006; **35**(11):1359–1379.
27. Dolsek M. Development of computing environment for the seismic performance assessment of reinforced concrete frames by using simplified nonlinear models. *Bulletin of Earthquake Engineering* 2010; **8**(6):1309–1329. DOI: 10.1007/s10518-010-9184-8.
28. Fardis MN (ed.). Experimental and numerical investigations on the seismic response of RC infilled frames and recommendations for code provisions. *ECOEST/PREC 8 Rep. No. 6*, LNEC, Lisbon, 1996.
29. Negro P, Pinto AV, Verzeletti G, Magonette GE. PsD test on four-story R/C building designed according to Eurocodes. *Journal of Structural Engineering* 1996; **122**(12):1409–1417.
30. Open System for Earthquake Engineering Simulation (OpenSees). Pacific Earthquake Engineering Research Center, University of California, Berkeley, CA, ⟨http://opensees.berkeley.edu/⟩ (Feb. 22, 2011).
31. Peruš I, Poljanšek K, Fajfar P. Flexural deformation capacity of rectangular RC columns determined by the CAE method. *Earthquake Engineering and Structural Dynamics* 2006; **35**(12):1453–1470. DOI: 10.1002/eqe.584.
32. CEN. Eurocode 8: design of structures for earthquake resistance - part 3: assessment and retrofitting of buildings, EN 1998–3. European Committee for Standardisation: Brussels, 2005.
33. Jayaram N, Lin T, Baker JW. A computationally efficient ground-motion selection algorithm for matching a target response spectrum mean and variance. *Earthquake Spectra* 2011; **27**(3):797–815.
34. Baker JW, Lin T, Shahi SK, Jayaram N. New ground motion selection procedures and selected motions for the PEER transportation research program. *PEER Report 2011/03*, University of California, Berkeley, 2011.